Kinetics of Steel Scrap Melting in Molten Fe-C Bath

Liviu C. Brabie and Masahiro Kawakami*

Graduate Course, Toyohashi University of Technology
Tempakucho-aza-Hibarigaoka, Toyohashi 441-8580, Japan
**Faculty of Engineering, Toyohashi University of Technology*

(Received November 2, 1998; final form December 24, 1998)

ABSTRACT:

The melting phenomena of steel scrap in molten steel bath has been investigated by several workers. Their works are reviewed in the present paper. The phenomena are, in general, so complicated that both heat and mass transfer take place simultaneously. Many workers made small scale experiments in such condition that only mass transfer was taken into consideration. The results were summarized in the form of dimensionless correlation among *Sh, Gr, Re, Sc* and J_D. Only one paper reported the experiment in which pure heat transfer was taken into consideration. The overall heat transfer coefficient was estimated by fitting numerical solution of heat transfer equations to the results of immersion experiments. The simultaneous heat and mass transfer were analyzed by mathematical model in relation to BOF converter operation. Some workers made experiments and numerical solution of mathematical model to obtain the heat and mass transfer coefficients in pilot plant converter and commercial converter.

1. INTRODUCTION

In the industrialized countries, steel products have been accumulated and the generation rate of steel scrap becomes very high. For example, in Japan, steel accumulation is anticipated as 1.3 bt and the generation rate, 57.5 mt in AC 2000. Therefore, it is desirable to utilize steel scrap from the viewpoint of energy and resource saving. Actually, the steel production by electric arc furnaces has increased during the last decade Also, many research and development works have been proceeding on how to utilize the steel scrap other than in electric arc furnace. In any case, scrap melting is the key technology and the melting phenomena should be investigated to acquire the optimum condition such as size and shape of scrap, their chemical composition, bath temperature and composition, degree of preheating and so on. Such needs arose about 40 years ago, at which time researchers wished to know how much scrap could be used in BOF converters.

There have been several papers to simulate scrap melting under converter operating conditions. For that purpose, the rate parameters such as heat transfer coefficient and mass transfer coefficient in various conditions were examined in small scale experiments. The pioneer work by Phelke *et al.* /1/ was published in 1965. They showed almost everything that would happen if cold steel scraps were dipped into high temperature melt, as will be shown in the following section. Since then, several works have been published on scrap melting, not only small scale experiments but also plant scale experiments and simulation works. They are classified 1) mass transfer experiments /2-7/, 2) heat transfer experiments /8-10/, 3) simultaneous heat and mass transfer experiments /1,9,11-14/, and 4) simulation in converter operation /12,14-17/. In the present paper, the above four categories are reviewed and what is understood up till now will be summarized.

2. PHENOMENOLOGICAL UNDERSTANDING OF COLD SCRAP MELTING IN STEEL MELT

Pehlke *et al.*/ 1/ made a small scale experiment with 90 kg bath (2.22 wt%< C< 4.18 wt%) in order to evaluate the rate of dissolution of steel bars in molten pig iron. They measured the rate of dissolution of AISI 1020 steel bars (with 1.3 to 5.1 cm diameters) in the temperature range of 1260 to 1454°C under different agitation conditions: namely, induction stirring by the furnace power, mechanical stirring + induction stirring, mechanical stirring with furnace power off, power off and no mechanical stirring.

Figure 1 shows the influence of the bath temperature on the dissolution of steel bars at two rate of stirring, as an example. At low temperature, the radius of steel bar grew up to a certain maximum value for short immersion time and then it decreased. The increase in radius is due to formation of solidified metal layer, crust. The crust was apt to be formed in the case of thicker steel bars. Under the normal operating conditions, however, the crust did not grow to a large thickness, and lasted only for a short time. The decrease in radius is due to dissolution or melting. Once the dissolution started, the radius decreased linearly with time. Thus, the dissolution rate was evaluated by the slope of line. Their results are summarized as follows.

1) If the specimen is large or temperature is low, the crust appears on the surface of steel bar to retard the dissolution.
2) The radius of the specimen decreases linearly with time.
3) The dissolution rate is high at high temperature, with strong stirring and high carbon content in the bath.

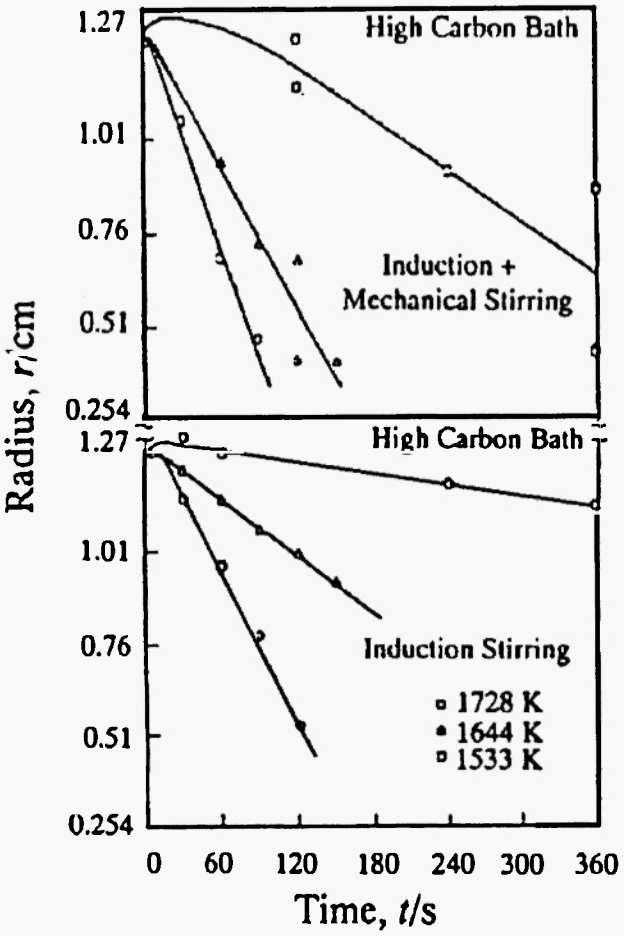

Fig. 1: Influence of temperature on the dissolution of 2.54 cm-diameter steel bars at two rates of stirring /1/.

3. THEORETICAL CONSIDERATIONS

The term of scrap melting is in fact a dissolution phenomenon in which heat and mass transfers between liquid and solid metal are taking place. It has been found that the melting rate of the scrap is dependent on the difference in carbon content between scrap and the melt. **Figure 2** shows the temperatures and concentrations profiles for melting of a solid into a carbon-saturated bath. The bath has the temperature T_L and the carbon concentration C_L. Prior to immersion, the temperature of the solid body is uniform at T_0, and after immersion, the surface acquires the temperature T_S lower than the bath temperature. At the surface of the scrap, the equilibrium concentration C_L^* for the temperature T_S is achieved in the liquid and the equilibrium concentration C_S^* in the solid. In general, T_L and C_L differ from T_S and C^*_L, respectively. Thus, heat and mass transfer take place through the boundary layer δ_T and δ_C, respectively. The boundary layer δ_T is related to δ_C, depending on fluid flow condition in the system. Even when the agitation of the fluid is violent, this layer does not disappear. Hence, the thickness and the characteristics of this boundary layer determine the heat transfer. Inside the solid, heat will be transported from the exterior towards interior sections of the rod bar solely by heat conduction. The general equation for heat

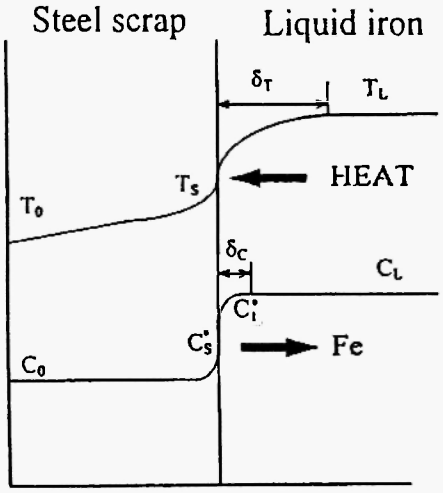

Fig. 2: Schematic diagram of heat and mass transfer between cold steel and hot bath.

conduction in solid can be written /18/ as:

$$\nabla k \nabla T = \rho \frac{\partial (C_p T)}{\partial t} \tag{1}$$

where ∇ is the three-dimensional differential operator. The more common form of this equation for cylindrical or spherical coordinate is:

$$\alpha \left(\frac{\partial^2 T}{\partial r^2} + \frac{n}{r} \frac{\partial T}{\partial r} \right) = \frac{\partial T}{\partial r}, \quad 0 < r < r(t) \tag{2}$$

where n = 1, 2 for cylinder and sphere respectively, r is radius and α is the thermal diffusivity ($\lambda/\rho C_p$). The equation for the conservation of heat connected with melting and solidification at solid – melt interface can be written as follows:

$$\lambda \frac{\partial T}{\partial r} = h\left(T_L - T_S\right) + \rho \Delta H \frac{dr}{dt} \tag{3}$$

where $\lambda \frac{\partial T}{\partial r}$ is the heat transferred into solid, $h(T_L - T_S)$ is the heat transferred from the bulk melt and $\rho \Delta H \frac{dr}{dt}$ is the latent heat for phase transformation. The other boundary conditions are as follows:

$$T = T_0 \qquad r, t < 0 \tag{4}$$

$$\frac{\partial T}{\partial r} = 0 \qquad r = 0, t > 0 \tag{5}$$

$$T = T_S \qquad r = r(t), t > 0 \tag{6}$$

Equation (6) states that the position of solid-melt boundary layer r(t) moves as the solidification or dissolution proceeds. Thus, r(t) is a function of time. Because the carbon concentration at the solid-liquid interface is time depending, also the melting point temperature must be time dependent.

To describe the rate of movement at the interface in a liquid-solid system for isothermal systems, the equation derived by Lommel and Chalmers /19/ may be used:

$$\frac{dr}{dt} = k_m \ln \left[1 + \frac{C_l - C_l^*}{C_l^* - C_s} \right] \tag{7}$$

where k_m is the mass transfer coefficient, defined as the D_{AB}/δ_C, the ratio of the diffusion coefficient to the diffusion boundary layer thickness. This equation assumed that the dissolution rates are controlled by the interdiffusion of iron and carbon in the liquid boundary layer and densities in the solid and liquid are equal. The values of mass transfer coefficient depend on the shape of the body, the nature of fluid flow around it and various physical parameters that include the diffusion coefficient.

A few obvious cases can be drawn:

Case 1: If the heat transfer is much faster than mass transfer and the carbon content in the solid steel is different from that of the melt, only mass transfer process should be considered.

Case 2: On the contrary, if the carbon content in the solid is equal to that in the melt, only the heat transfer should be considered.

Case 3: In general, both transfer processes should be considered simultaneously. In this case, the carbon content of the solid surface should be related to the temperature, referring to the binary-phase diagram of Fe-C.

$$C_l^* = f(T_S) \tag{8}$$

4. MASS TRANSFER

4.1 Dissolution under natural convection

Static methods are obviously the easiest way to study interactions in solid-liquid systems, since they require a minimum of apparatus. According to the assumption that the mechanism of scrap dissolution is based on the diffusion of carbon from bath to the steel bar, one might predict that melting rates in a stagnant bath must be notably low. This prediction is not correct because the stagnant condition cannot exist in the vicinity of the melting interface due to the natural convection currents created by the difference in density in the bulk liquid (high C) and the melting interface (low C). Kosaka and Minowa /3/ reported that the shape of the bar was of a frustum cone in stagnant melt. The explanation for this shape is given by the change in dissolution rate along the rod bar. The liquid beside the bar would descend along the surface. The boundary layer would become thicker at the lower part of the bar, and thus the dissolution rate would become smaller. Because of the difference between the diameters along the rod bar, the diameter or radius at the middle was used thereafter.

Kim and Pehlke /5/ carried out dissolution experiments on a vertical cylinder (1.27 cm diameter made by Ferrovac E and/or 1045 steel) into a static bath under isothermal conditions. They used a resistance-heated furnace with a vertically mounted mullite tube, power control unit, a specimen holding assembly and a gas train. After immersion in the bath, the shape of the rod was of a frustum cone, which was seen in the work by Kosaka and Minowa /3/. In **Fig. 3**, the changes in diameters were plotted against the immersion time at each temperature for dissolution of a Ferrovac E into the carbon saturated liquid iron bath. The rates of dissolution were usually assessed by the rate of change of the rod diameters and depended on how quickly carbon could be transported to the interface. Mass transfer coefficients can be derived from the slope of the lines using the Lommel and Chalmers equation, Eq (7). The dissolution rates increase strongly with increasing melt temperature.

Wright /7/ studied the dissolution rates for solid steel cylinders ranging from 8 to 12 cm length and 1.21 cm in diameter immersed in a stagnant bath under isothermal

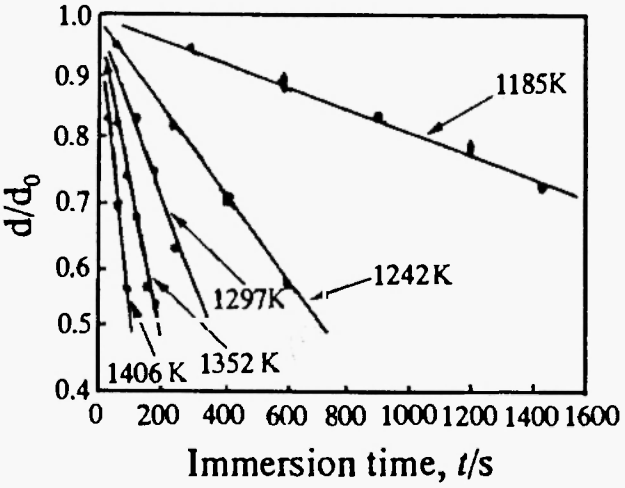

Fig. 3: Stationary dissolution of Ferrovac E into carbon-saturated liquid iron bath /5/.

conditions. The bath carbon content ranged from 2 to 4.5 wt% and bath temperature from 1260 to 1460°C. **Figure 4** shows the effect of carbon content in the bath at 1460°C on the dissolution rates of the bars. The rod diameters versus immersion time plots are linear and the dissolution rates increase with increasing carbon content in the bath.

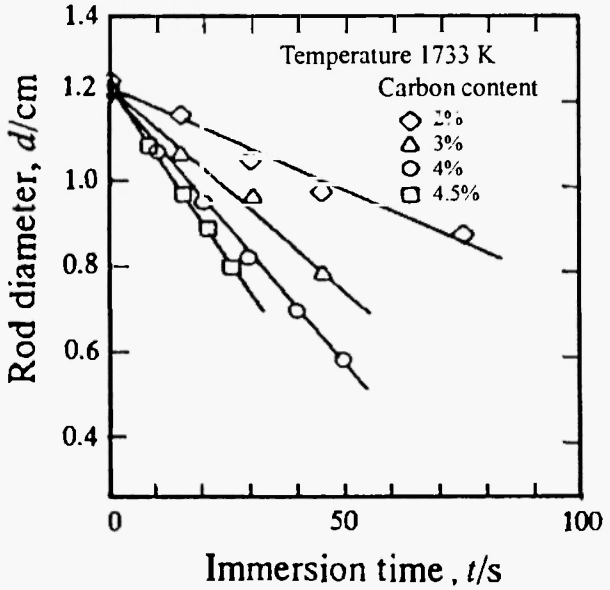

Fig. 4: Effect of carbon content on the dissolution of rods under natural convection conditions /7/.

Kosaka and Minowa /3/ obtained similar results. Nomura and Mori /4/ carried out a unique experiment.

where the Fe-C melt was put on solid iron. The dissolution rate was monitored by the change in carbon content in the melt. They estimated the thickness of boundary layer for mass transfer as 5×10^{-5} to 10^{-4} m at 1200 to 1400°C.

Table 1 shows the results obtained by various researchers for dissolution experiments under stagnant conditions. It may be noted that the experimental mass transfer coefficients are in good agreement. An estimation of melting times is obtained from extrapolation of the corresponding linear plot of diameters to zero. The results confirm the influence of increasing bath temperature and increasing bath carbon content on shortening melting times. For example, an increase in bath carbon from 2.1 to 4.71 wt% decreases melting time for the same rod from 3000 to 500 seconds.

In general, a dimensionless correlation is derived to summarize experimental results under wide conditions. The convection mass transfer data can be correlated in terms of dimensionless numbers of the Sherwood ($Sh = \frac{k_M L}{D_{AB}}$), Reynolds ($Re$), Schimdt ($Sc = \frac{\nu}{D_{AB}}$), Grashof ($Gr_m = \frac{\rho_l(\rho_l^* - \rho_l)gL^3}{\mu^2}$) and Raleigh ($Ra$) numbers. The characteristic length L is the diameter for circular geometries such as cylinders and spheres, μ is the viscosity of the liquid, ν is the kinematic viscosity, ρ_l and ρ_l^* is the density of bulk liquid and density of the liquid iron-carbon alloy respectively.

A dimensionless correlation of Nusselt type can be used for the mass transfer with natural convection:

$$Sh = a(Gr_m Sc)^n \tag{9}$$

The dimensionless correlation obtained by Kim and Pehlke /5/ for mass transfer with natural convection ($60<Sh<120$ and $6.9\times10^8<Gr_mSc<7.7\times10^9$) is as follows:

$$Sh - 0.149\,(Gr_m\,Sc)^{0.294} \tag{10}$$

The linear regression analyses obtained by Wright /7/ for a turbulent natural convective flow ($142<Sc<195$ and $Gr_mSc>10^9$) gives:

$$Sh = 0.13\,(Gr_m\,Sc)^{0.34} \tag{11}$$

Kosaka and Minowa /3/ obtained the following relation ($10^9<Gr_mSc<10^{11}$):

$$Sh = 0.11(Gr_m\,Sc)^{1/3} \tag{12}$$

These relations are shown in **Fig. 5**. As seen in the figure, Eqs. (11) and (12) agree with each other. Although Eq. (10) is slightly smaller than the others, the exponent in the equation is nearly the same as the others. Equations (10) to (12) provide a convenient

Table 1

Reported values for mass transfer coefficients and melting times for static systems

Initial Diameter (cm)	Bath Temperature (°C)	Sample Carbon (wt%)	Bath Carbon (wt%)	Experimental mass transfer coefficient (cm/sec)	Melting time (sec)
1.21[7]	1400	0.26	4	3.8×10^{-3}–4×10^{-3}	(170)
1.27[5]	1241	0.44	C sat. iron	1.825×10^{-3}	(1128)
2.54[1]	1371	0.2	3.84	0.99×10^{-3}	(1380)
2.54[11]	1482	0.1	4.74	1.23×10^{-3}	150
3.81[11]	1482	0.1	4.74	1.15×10^{-3}	240
5.08[11]	1482	0.1	4.74	1.23×10^{-3}	300
7.62[11]	1471	0.1	4.71	1.46×10^{-3}	480
7.62[11]	1431	0.1	2.1	1.59×10^{-3}	3000

( ) = extrapolated.

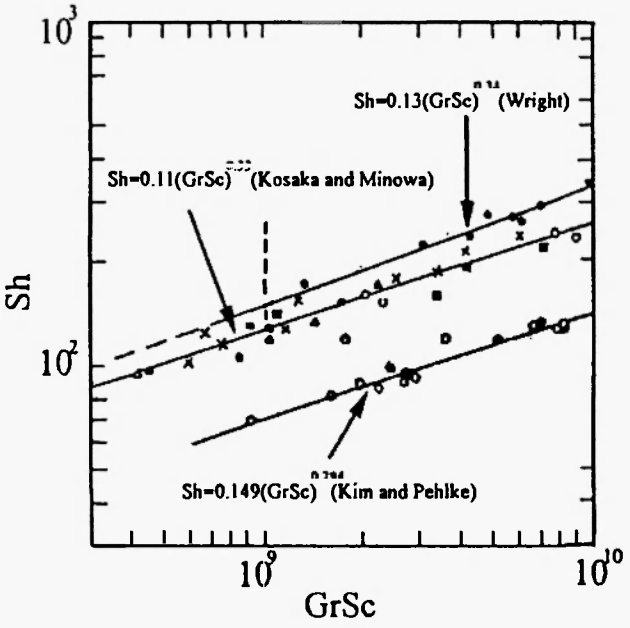

Fig. 5: Mass transfer correlation for dissolution from a stationary specimen /3,5,7/.

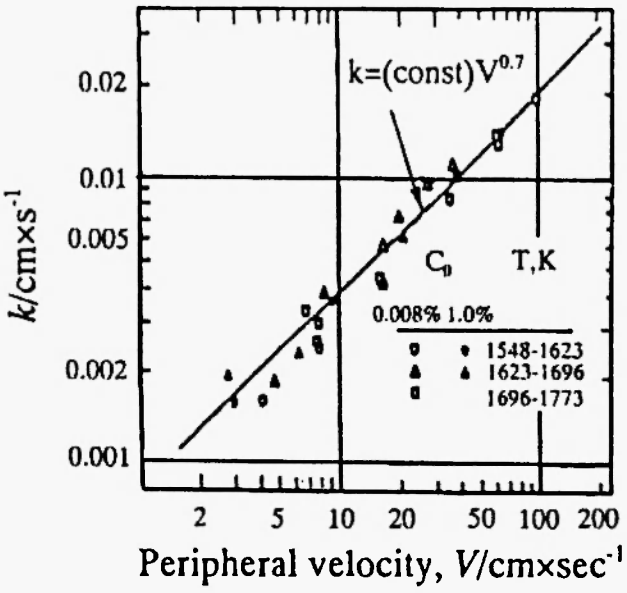

Fig. 6: Experimental mass transfer coefficient vs. peripheral velocity for dissolution of carbon steel in saturated Fe-C alloy /2/.

method for calculating mass transfer coefficients under turbulent natural convection conditions.

4.2 Dissolution under forced convection

Rotating specimen

Olsson *et al.* /2/ studied the rates of dissolution of cylindrical iron-carbon samples with 1.9 cm diameters and 0.0081 or 1.0 wt% C in a 1200 g carbon saturated iron bath under isothermal conditions at 1274 to 1500°C. The alloy was kept under argon atmosphere in the graphite crucible heated up by an induction coil. The samples were preheated to ca. 100°C lower temperature than the bath temperature before immersion. The rotation speed, obtained by a variable-speed motor, was in the range of 32 to 1210 rpm for 25 to 120 sec. The radius decreased uniformly along a vertical axis. It decreased linearly with time, which is the same as in the case of stagnant condition. From the slope of the line, the mass transfer coefficient was obtained using Eq. (7). They obtained a correlation between mass transfer coefficient and peripheral velocity, as can be seen in Fig. 6:

$$k_m = (const) V^{0.7} \qquad (13)$$

Kim and Pehlke /5/ derived the similar correlation between the mass transfer coefficient and the fluid velocity, u as

$$k_m = constant\ (u)^{0.670} \qquad (14)$$

In this kind of experiments, the results are usually summarized by correlating J_D-factor for mass transfer and Reynolds number, where J_D-factor is defined by:

$$J_D = \frac{k_m}{u} Sc^{0.644} \qquad (15)$$

Kim and Pehlke /5/ derived the correlation for a rotated specimen in the range of 450 to 1800 rpm. They can be expressed in the form:

$$J_D = 0.112 Re^{-0.330} \qquad (16)$$

Kosaka and Minowa /3/ obtained the following results (10^2<Re<10^4, 1300~1500 °C):

$$J_D = (k/u) Sc^{2/3} = 0.064 (Re)^{-0.25} \qquad (17)$$

This result is slightly different from that by Kim and Pehlke /5/, as shown in **Fig.** 7.

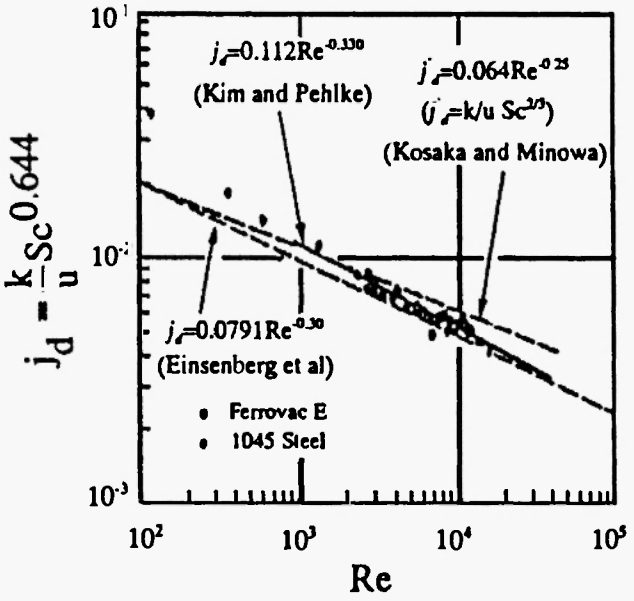

Fig. 7: Relation between mass transfer J-factor and Reynolds number for rotational dissolution of iron cylinder into molten carbon-saturated iron /3,6/.

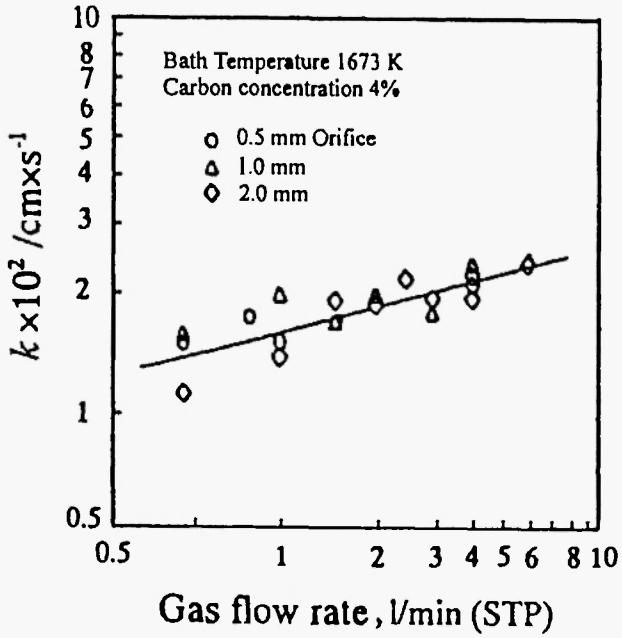

Fig. 8: Plot used for the regression analyses of the mass transfer with gas flow rate /7/.

Gas stirred systems

Gas injection technique into a liquid bath has been of considerable importance in high temperature metallurgical processes. The main purposes for the gas injection include acceleration of mass transfer and homogenizing the liquid bath in concentration and temperature. When gas is injected through a bottom nozzle at a high gas flow rate, it provides effective stirring of the bath. Wright /7/ measured the dissolution rates of the bars immersed into a 1 kg and 25 kg iron-carbon bath under various gas flow/orifice size conditions. The plots of the diameters versus immersion time show that the dissolution rates increase with increasing gas stirring flow rates. The mass transfer coefficients, obtained from the dissolution rates in the same procedure as above, are plotted against the gas stirring flow rates in Fig. 8. The relation between the mass transfer coefficients and the gas injection flow rate is expressed as:

$$k_m \propto (Q)^{0.21} \qquad (18)$$

Table 2 shows the coefficients of mass transfer and melting time for dissolution under different agitation conditions. Another point to note is the sensitivity of melting time and mass transfer coefficients on bath temperature and bath conditions. They can vary significantly. For example, the melting time is shortened for the same rod bar from 2200 to 100 seconds with increasing rotation speed from 20 rpm to 1800 rpm and temperature from 1247°C to 1406°C.

CO evolution

Mori and Sakuraya /6/ studied, in an indirect way, the effect of gas stirring on dissolution rates of cylindrical iron specimens with various amount of oxygen (O<1.14 %) into molten carbon-saturated iron alloys. During the dissolution process, the oxygen from specimen will enter to react with carbon in the melt and at the interface, the CO bubbles will be formed. According to their results, in a stationary bath, the oxygen content has an important role in dissolution rate, accelerating the process. The dependence of coefficient of mass transfer on oxygen content at different temperatures is shown in Fig. 9. At higher temperatures, the mass transfer coefficient increases with increasing the oxygen content. This is due to the enhanced mass

Table 2
Reported values for the coefficients of mass transfer and melting time for different bath conditions

Initial Radius (cm)	Bath temperature (°C)	Sample Carbon (wt%)	Bath Carbon (wt%)	Bath conditions	Experimental mass transfer coefficient (cm/sec)	Melting time (sec)
2.54[1)]	1371	0.2	4.14	Inductively stirred	2.38×10^{3}	(505)
1.27[5)]	1247	0.007	C sat. iron	Stirring (20rpm)	2.137×10^{3}	(2184)
1.27[5)]	1406	0.007	C sat. iron	Stirring (1800rpm)	38.12×10^{3}	(99)
1.21[7)]	1400	0.26	4	Gas stirring (6l/min)	24.5×10^{3}	(25)

( ) = extrapolated

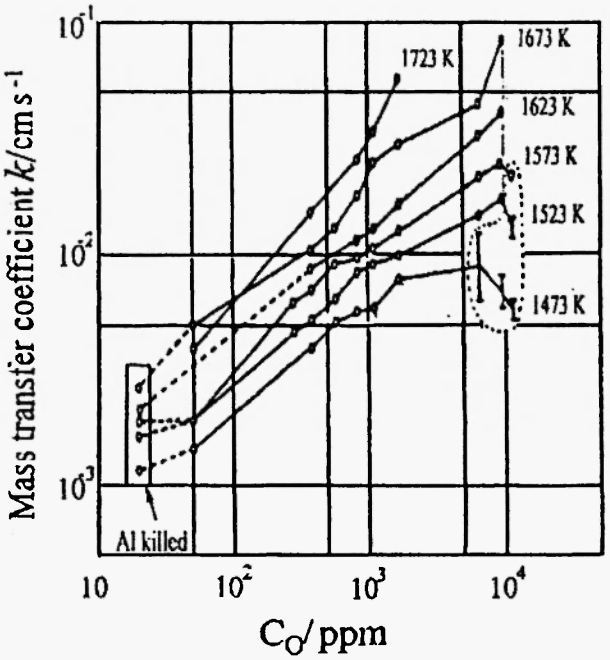

Fig. 9: Mass transfer coefficient versus oxygen concentration for stationary dissolution at various temperatures /6/.

transfer by the formation of fine CO bubbles. On the contrary, at lower temperature and high oxygen content, the coefficient decreased as shown in the circled area by a broken line. This is due to the surface coverage by large bubbles. The correlation between the volumetric evolution rate of *CO*, V_{CO}, and the dissolution rate ($-dr/dt$) may be obtained from:

$$V_{CO} = \rho_{iron} \times (ppmO) \times 10^{-6} \times \left(-\frac{dr}{dt}\right) \times \frac{1}{16} \times 2.24 \times 10^{4} \times \left(\frac{T+273}{273}\right) \quad (19)$$

where ρ_{iron} is density of solid iron (g/cm^3) and T, the experimental temperature (°C). The mass transfer coefficient is plotted against V_{CO} in Fig. 10. At the temperatures below 1350°C, the mass transfer coefficient is proportional to $V_{CO}^{0.2}$ and at the temperatures of 1350 to 1450°C, to $V_{CO}^{0.45}$.

The effect of rotation of specimen was compared to that of CO evolution in carbon saturated iron bath at 1250°C. At lower rpm, the mass transfer coefficient is controlled mainly by the amount of CO, but the effect of rotation become predominant for rpm > 250.

Iron spheres are of great interest because the use of sponge pellets has begun to increase in the production of steel. Seaton *et al.* /13/ studied the rate of dissolution of sponge iron pellets with various oxygen content into molten steel. The pellets also have a higher carbon content than the melt. In this case, the carbon in pellets reacts with oxygen to form CO bubbles, which are

expected to accelerate the dissolution.

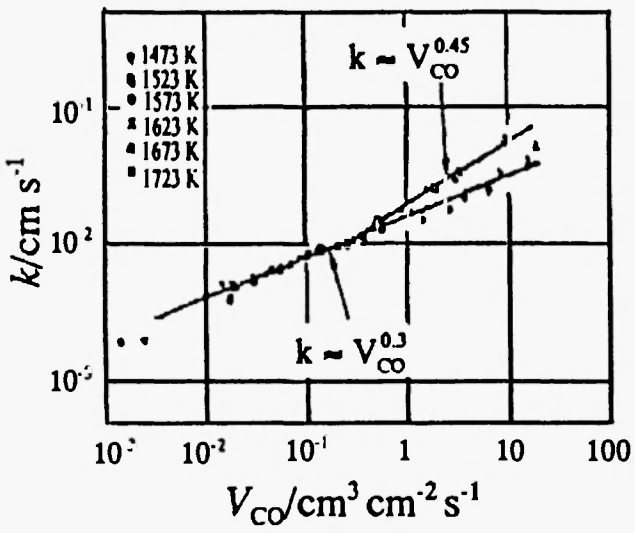

Fig. 10: Mass transfer coefficient versus CO evolution rate for stationary dissolution at various temperatures /6/.

5. HEAT TRANSFER

By application of Green's functions method, Ehrich *et al.* /9/ solved the equations from (2) to (6) for obtaining the melting behavior of sponge iron pellets in an iron bath. In equation (2), n was taken as 2. In order to check the theoretical assumptions, experiments were carried out with spherical specimens in an induction furnace of 20-kg capacity under argon atmosphere. Alumina markers were inserted at different depths inside the spheres to detect the melting position at a proper time. For the model proposed, the solid crust formation at short-time immersion was taken into account. The different compositions of the crust from sponge iron pellets were also taken into account. Figure 11 shows that the computational results are in close agreement with experimental values, assuming heat transfer coefficient h of 0.78 cal s^{-1}cm^{-2} K^{-1}. So the model was proved to be reliable. Then, the model examined the effect of several parameters on dissolution behavior. The results of the examination are summarized as follows: The crust cannot reach more than 10% of the initial radius and it exists just for a short time. The melting curve is not linear but convex. The melting rate is higher with higher super heat. The

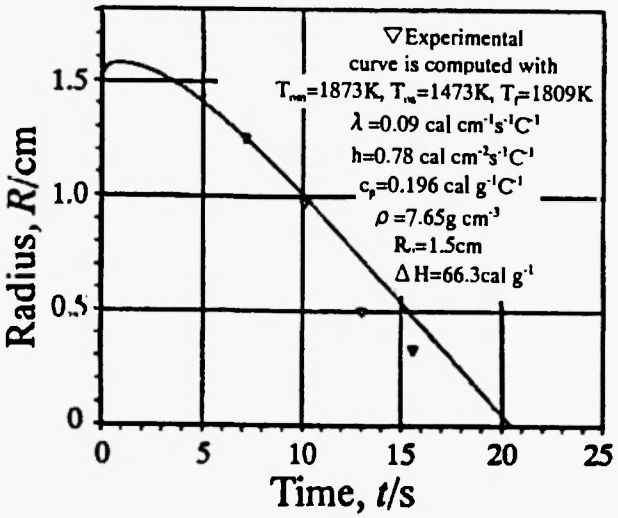

Fig. 11: Radius of dense iron sphere submerged into liquid iron at 1873K, as function of time /9/.

coefficient of heat transfer of 0.8 cal s^{-1}cm^{-2} K^{-1} for dense spheres preheated up to 1200°C is more reliable than 0.25~0.5 cal s^{-1}cm^{-2} K^{-1} obtained for pellets with initial temperature T = 30°C immersed into liquid iron. They explain this difference by the dependence of thermal conductivity and/or specific heat on temperature, although constant values were used in their computation.

Guthrie and Gourtsoyannis /8/ developed a heat transfer model (based on finite-difference equations) in order to obtain the melting time of iron spheres (≈ 0.85 wt%C) of various size in a stagnant iron bath which was saturated with carbon. In their model, the heat transfer coefficient was assumed using the following dimensionless relation:

$$Nu=0.53(GrmPr)^{1/4} \qquad (20)$$

They analyzed the effects of sphere size, preheat, melting point and bath temperature on dissolution kinetics, factors which are in strong correlation regarding the time necessary for a complete melting. For example, Fig. 12 shows melting time of iron spheres. The experimental values are about 25% less than those computed for some reasons of experimental complications. The preheating temperature can play an important role in the decrease in melting time. More exactly, for a 580°C preheat temperature of the 6.5 cm

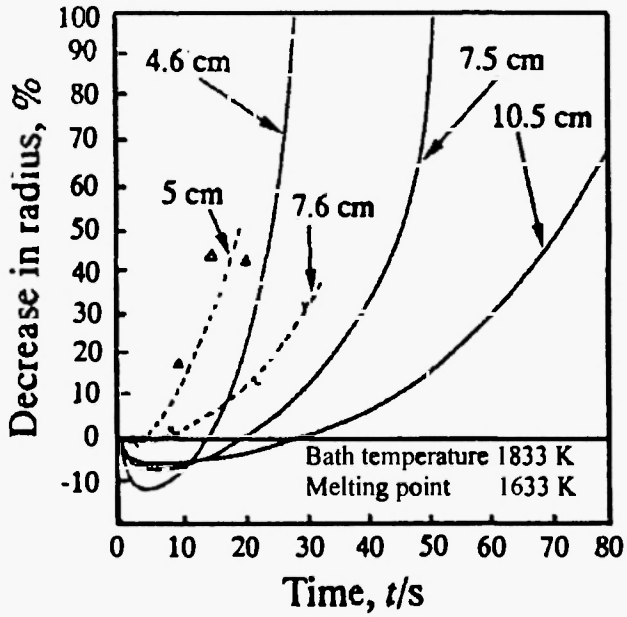

Fig. 12: Plot of predicted and experimental changes in radius with immersion time for spheres of various diameters /8/.

diameter iron spheres immersed into the molten bath at 1640°C, the melting time is reduced by 25%. The effect of superheat temperature on melting rate was such that at superheat temperature in excess of about 50°C, the melting time decreased substantially. For melting time of iron spheres of small radius, the results are in good agreement with those obtained by Ehrich *et al.* / 9/.

6. HEAT AND MASS TRANSFER

Szekely *et al.* /12/ examined the kinetics of scrap melting by the mathematical model and experiments. In the experiments, an induction furnace with 295 kg capacity was used. The bath carbon content varied from 2.4 to 4.4 wt%. The bar diameters ranged from 1.9 to 11 cm. The immersion time ranged from 15 to 330 seconds. In their model, equations similar to Eqs. (2) to (6) were used to describe heat transfer. For the description of mass transfer, however, Eq.(21) was used instead of Eq. (7):

$$C_L^* = \frac{k_m\left[C_L - C_L^*\right]}{\left(\frac{dr}{dt}\right) + k_n\left[C_L - C_L^*\right]} \qquad (21)$$

The equation (8) was converted to explicit function as

$$T_S(^0F) = 2800 - 1.5\times10^4 C^*_L, \quad 0 < C^*_L < 0.04 \qquad (22)$$

Assuming turbulent flow, the coefficient of mass and heat transfer were correlated by

$$\frac{h_D}{h} = Sc^{1/3}Pr^{-0.8}\frac{D}{k} \qquad (23)$$

where D is the inter-diffusivity of Fe and C. This system of equations was solved by manipulation of Green's function. Figure 13 shows the melting process of rods of 1.9 cm initial radius. The solid triangles represent the experimental data points and the curves correspond to the calculated time-dependent position of the melt-rod interface. As can be seen from the figure, the calculation gives a good prediction of melting process by taking appropriate heat transfer coefficient of 3,500 $Wm^{-2}K^{-1}$. The solidified crust formed on the cylinder for short immersion time was reported and also taken into account for computational model. The heat transfer coefficient between melt and rod for stirring conditions was determined by fitting the results of numerical analyses to those of experimental measurements. The

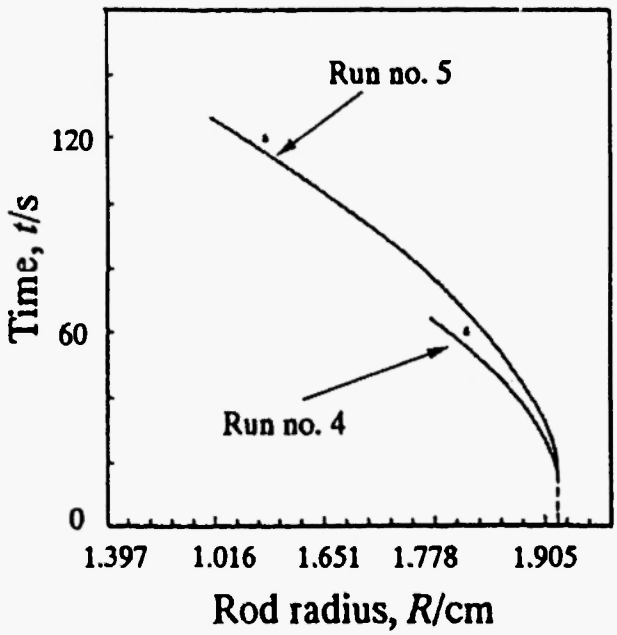

Fig. 13: Progress of melting as indicated by computed curves and measured points, for runs No. 4 and 5 /12/.

coefficients range between 3,500 to 11,800 $Wm^{-2}K^{-1}$.

Guthrie and Stubbs /11/ made some experiments under conditions where both heat and mass transfer should be taken into account. In reality, however, they analyzed the data only by mass transfer. The steel bars of different radius were immersed to the carbon saturated melt of 227 kg under stagnant conditions. The decrease in radius was estimated by the weight loss. The mass transfer coefficient was experimentally obtained by the following equation:

$$k = \frac{\frac{\rho}{\rho^*} C_L^* - C_0}{C_L - C_L^*} \tag{24}$$

The mass transfer coefficient, k_E, was predicted using the dimensionless correlation of:

$$Sh = 0.13 (Grm\ Sc)^{1/3} \tag{25}$$

They concluded that k is 0.30~0.60 times k_E.

Seaton *et al.* /13/ obtained the heat transfer coefficient as a function of the radius of the pellet by the curve fitting of the calculated results of the temperature at the pellet center to those of the experimental measurement. An example is shown in Fig. 14. They used a similar analytical method to that of Szekely *et al.* /12/. The coefficient of mass transfer tried was in the range of 0.20 to 0.60 cal $s^{-1}cm^{-2}K^{-1}$. But there are still some discrepancies, caused by the changes in the physical properties of the pellets during the melting process. The cross-sections of pellets which were dipped into the melt and withdrawn were analyzed by scanning electron microscopy in order to determine the structural changes occurring during the melting process. The results showed that the oxide phases were reduced with a continuous gas evolution of 150 and 280 cm^3 in Midrex and HyL pellets, respectively, and that the gas evolution accelerated the melting process.

When a cold steel bar is dipped into the iron melt, crust formation has been reported by several workers /1,9,12,13/. In many cases of crust formation, an air gap is apt to be formed. Isobe *et al.* /14/ took into account heat transfer resistance at the gap when making their mathematical model, although others did not take this factor into account. They made a similar experiment to that of others /2,5/ with a rotating specimen. The mathematical model was composed exclusively of Eqs. (2) to (8). The equations were numerically solved by computer, introducing a new heat transfer coefficient of hc at the gap. Figure 15 shows an example of the result.

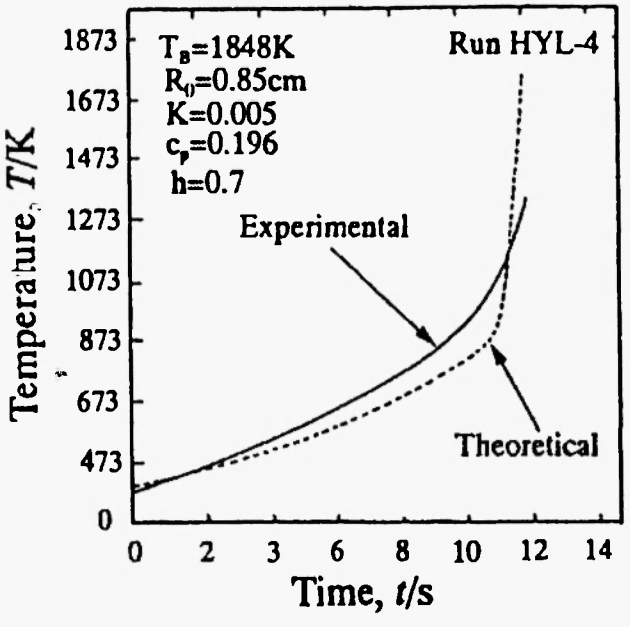

Fig. 14: Temperature versus time at the center of an HyL pellet immersed in liquid steel at 1848 K /13/.

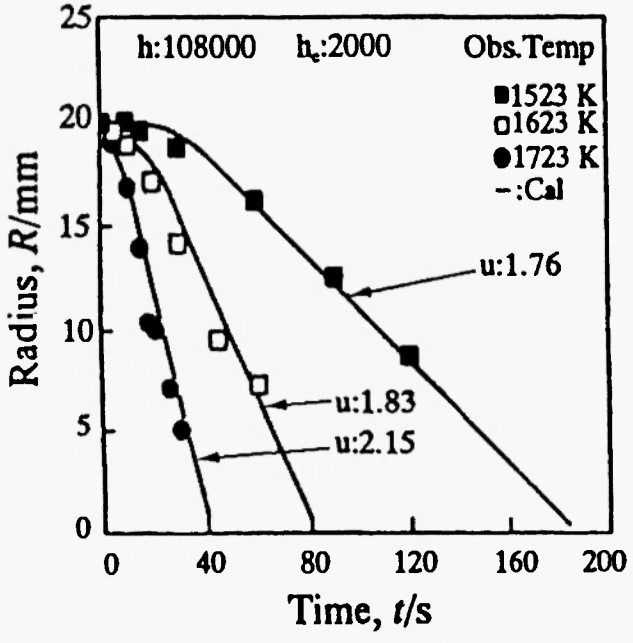

Fig. 15: Change of radius of carbon steel rod immersed in liquid Fe-C /14/.

The plots are the experimental results and the curves are the results of computation where heat transfer coefficient between melt and steel bar, h, and the coefficient at the gap, hc, were assumed as 108,000 and 2,000 $Wm^{-2}K^{-1}$, respectively. The symbol u in the figure is the mass transfer coefficient which corresponds to k_m in Eq. (7). The dimensionless correlation for mass transfer was given as:

$$Sh=0.163Re^{0.78}Sc^{0.356} \quad (26)$$

7. ANALYSIS OF CONVERTER OPERATION

During converter operation, the bath temperature is as low as 1350°C at the starting point and increases gradually up to 1700°C. On the contrary, the carbon content decreases from C ≈ 4.5 wt% to less than 0.1 wt%. In order to simulate converter operation, both T_L and C_L in Fig. 2 should be time dependent. For such situations, several workers /12,14-17/ have tried to predict the melting rate of scraps.

Mori and Nomura /15/ simulated the scrap melting in a converter with a value of boundary layer thickness of their own to examine the effect of several parameters such as shape and size of scrap, blowing pattern and so on. One of their conclusions is that the melting process of thin plate is controlled by mass transfer, while that of thick plate is controlled by both heat and mass transfer. Asai and Muchi /16/ simulated the converter operation based on a T – C (temperature – carbon content) diagram. The effect of scrap addition on the operation was examined with their mathematical model which was based on heat and mass balance between solid phase and the melt. It is concluded that the scrap addition affected very much on converter operation and the relation between temperature and carbon content during the operation moved closely to the liquidus line on the T – C diagram. Finally, a method of the end-point dynamic control with the aid of a topological phase diagram was proposed. Szekely *et al.* /12/ developed the analytical method of scrap dissolution described in the preceding section and applied it to the analysis of converter operation. Some of the results are as follows: the scrap melting which is facilitated by carbon diffusion from the melt to the scrap begins very early in the process. The melting is retarded and even terminated during the blow when the bath has insufficient superheat to provide the necessary sensible and latent heat for melting. The rate of scrap melting is accelerated if the carbon removal is retarded or if the temperature of the bath is increased rapidly to maintain a high level of superheat during blowing.

In the preceding works by Szekely *et al.* /12/, one of the most important parameters of heat transfer coefficient was estimated from small scale experiments. Recently, Gaye *et al.* /17/ made some plant scale experiments to determine the melting time of scrap. The experiments were performed in three commercial converters:

- LD converter: 310 t capacity without inert gas stirring during the oxygen blow.
- LET converter: 310 t capacity and combined blowing.
- LWS converter: 240 t capacity and bottom blowing.

Low carbon steel scraps with a capsule of 20 mm diameter containing activated Xenon were placed in the converters. The shape of the scrap piece was of a cylinder or a plate. The melting time at the depth of capsule position was detected by the emission of the Xenon to the exhausted gas. The results are shown in Fig. 16 in which experimental melting time is plotted against the scrap equivalent thickness. The authors

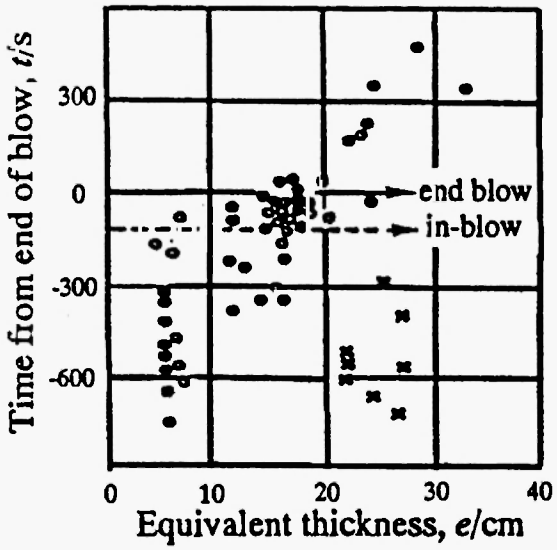

Fig. 16: Experimental results of scrap melting time in converters. Each point represents the experimental melting time of scrap, referred to end of main blow, versus its equivalent thickness /17/.

observed that the melting time of pig iron plate is shorter than low carbon scrap and the blowing conditions cannot drastically affect the melting time. Moreover, there is a significant scatter caused by cold scrap characteristics and timing of in-blow addition of iron ore. A similar analytical method to that by Szekely *et al.* /12/ was adopted to obtain the heat transfer coefficients. They were determined by fitting the computed curves to the experimental results. Figure 17

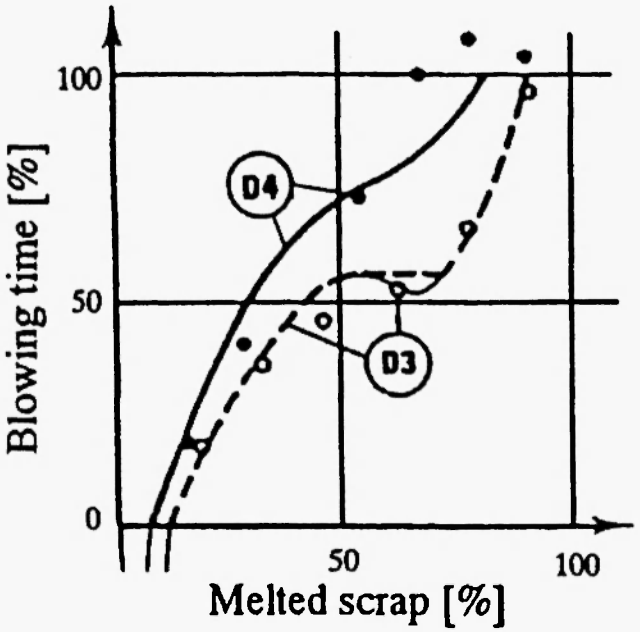

Fig. 17: Application of scrap melting algorithm to experimental results /17/.

shows two examples of the plot of % melted scrap versus blowing time. The smooth and dashed lines are computed results and the points are experimental results. From this figure, the heat transfer coefficient was estimated as 17,000 $Wm^{-2}K^{-1}$. The heat transfer coefficient for the respective converter are as follows:

- 17,000 W m^{-2} K^{-1} for LD
- 25,000 W m^{-2} K^{-1} for LET
- 50,000 W m^{-2} K^{-1} for LWS

The heat transfer coefficient is correlated to the average mixing power as :

$$h = 5000\ \varepsilon^{0.2} \qquad (28)$$

where h is the heat transfer coefficient and ε is the average mixing power in Wm^{-3}. They simulated the converter operation with this model. Some of conclusions are as follows: the admissible limits of scrap thickness are much more stringent when the complete melting is required at the time of in-blow sublance sampling rather than at the blow end. There is more flexibility in scrap melting when the hot metal ratio in not too low. The preheating of heavy scrap does not appreciably speed up its melting.

Isobe *et al.* /14/ made the experiments with 5 t pilot converter to evaluate the heat and mass transfer coefficients in the furnace. The pulverized coal and oxygen were injected from the bottom and oxygen was top blown by the top lance to supply the necessary heat. Cubic scrap of 1 to 2.4 t was charged to the furnace. The scrap melting was monitored by the copper balance in the furnace. Figure 18 shows an example of the results.

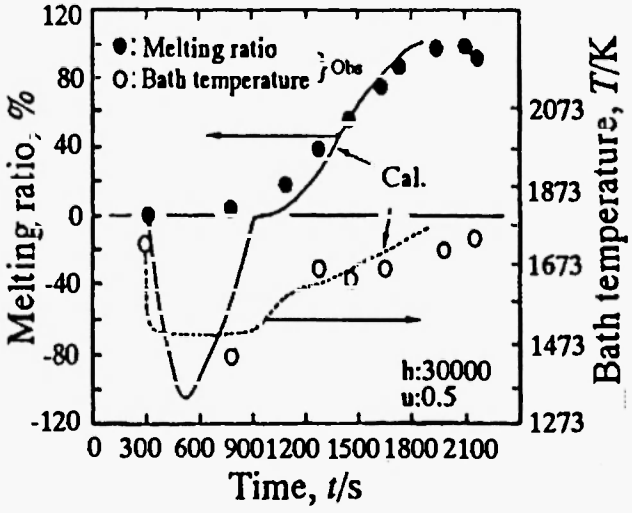

Fig. 18: Change of melting ratio and bath temperature as the time proceeds (5 t plant furnace) /14/.

The plots are the experimental result and the curves are the results of simulation analysis in which heat transfer coefficient and mass transfer coefficient were estimated as 30,000 $Wm^{-2}K^{-1}$ and as 1.4×10^{-4} m/s, respectively. The heat transfer coefficient ranges from 23,000 to 46,000 $Wm^{-2}K^{-1}$ at the average mixing power, ε, ranging from 3,500 to 12,000 Wt^{-1}. Using the simulation model shown in the preceding section with these parameters, the converter operation was analyzed. The results are summarized as follows: Increase of mixing power is effective foı reducing melting time but is not so

Table 3
Reported values for the heat transfer coefficients

Type of Experiment	Author	Heat Transfer Coefficient
Small scale experiment	Guthrie and Gourtsoyannis[8]	$Nu=0.539[Pr(Gr\ Pr)/(0.952+Pr)]^{1/4}$
	Szekely *et al.*[12]	3500~11800 W/m^2K
	Ehrich *et al.*[9]	32000 W/m^2K
	Isobe *et al.*[14]	5800~117000 W/m^2K
5 tone Convertor	Isobe *et al.*[14]	23000~46000 W/m^2K
		$h=4800\varepsilon^{0.2}$
Commercial Convertor	Gaye *et al.*[17]	17000~50000 W/m^2K
		$h=5000\varepsilon^{0.2}$

effective beyond a certain range. For stable operation, melting in the iron with high carbon content is preferable with respect to bath solidification. Increase of charging rate of scrap improves the productivity of the scrap melting process, within the range where excess solidification of melt does not occur.

Although the data of heat transfer coefficient are few, they are summarized in Table 3, including the data both from small scale experiments and from plant experiments.

8. CONCLUDING REMARKS

In general, scrap melting is a complicated process including simultaneous heat and mass transfer. In the case that the temperature of the melt is lower than the melting point of scrap, but the carbon content is higher in the melt than scrap, the melting is exclusively controlled by the mass transfer. Many small scale experiments have been carried out, and the mass transfer coefficients are summarized in the dimensionless correlation under natural and forced convective conditions. The sole heat transfer experiment seems difficult to perform, and only one paper has been reported. Some simultaneous heat and mass transfer experiments have been tried. In this case, the mathematical model seems difficult to make. In particular, how to estimate the heat transfer resistance at the air gap between scrap and crust still seems an unsolved problem. The data of heat transfer coefficient are still insufficient. As a whole, the quantitative analysis of individual cases is still open to question, although the analytical method with mathematical models has been established.

REFERENCES

1. R.D. Pehlke *et al.*, *Trans. Met. Soc. AIME,* **233,** 1420 (1965).
2. R.G. Olsson *et al.*, *ibid.*, **233,** 1654 (1965).
3. Mineo Kosaka & Susumu Minowa, *Tetsu-to-Hagane*, **53**, 983 (1967).
4. Hiroyuki Nomura & Kazumi Mori, *ibid.*, **55**, 1134 (1969).
5. Yeong-U Kim & Robert D. Pehlke, *Met Trans.*, **5**, 2527 (1974).
6. Kazumu Mori & Toshikazu Sakuraya, *Trans. ISIJ*, **22**, 984 (1982).
7. J.K. Wright, *Met. Trans B*, **20B**, 363(1989).
8. R.I.L. Guthrie & L. Gourtsoyannis, *Can. Met Qtry*, **10**, 37 (1971).
9. Olaf Ehrich *et al.*, *Arch. Eisenhüttenws.*, **50**, 329(1979).
10. Eckehard Specht & Rudolf Jescher, *Steel Research*, **64**, 28 (1993).
11. R.I.L. Guthrie & P. Stubbs, *Can. Met Qtry*, **12**, 465 (1973).
12. J. Szekely *et al.*, *Met Trans.* **3**, 1825 (1972).
13. Carlos E. Seaton *et al.*, *Trans. ISIJ*, 23, 14 (1993).
14. Kohichi Isobe *et al.*, *Tetsu-to-Hagane*, 76, 2033

(1990).
15. Kazumi Mori & Hiroyuki Nomura, *ibid.*, **55**, 347 (1969).
16. Shigeo Asai & Iwao Muchi, *ibid.*, **56**, 546 (1970).
17. H. Gaye *et al.*, *Steelmaking Conf. Proc.*, **68**, 91 (1985).
18. Hou-Cheng Huang & Asif S. Usmani, *Finite Element Analysis For Heat Transfer*, 15, Springer- Verlag, London (1994).
19. J.M. Lommel & B. Chamers, *Trans. Met. Soc. AIME*, **215**, 499 (1959).